ACS Macro Letters

Letter

pubs.acs.org/macroletters

Elucidation of the Chain-Folding Structure of a Semicrystalline Polymer in Single Crystals by Solid-State NMR

You-lee Hong and Toshikazu Miyoshi*

Department of Polymer Science, The University of Akron, Akron, Ohio 44325-3909, United States

Supporting Information

ABSTRACT: Despite tremendous efforts over the last half-century to elucidate the chain-folding (CF) structure of semicrystalline polymers, the re-entrance sites of folded chains, the successive CF number n, and the adjacent re-entry fraction F have not been well characterized due to experimental limitations. In this report, $^{13}C-^{13}C$ double-quantum (DQ) NMR was used to determine for the first time the detailed CF structure of ^{13}C CH_3-labeled *isotactic* poly(1-butene) (*i*PB1) in solution-grown crystals blended with nonlabeled *i*PB1 across a wide range of crystallization temperatures (T_cs). Comparison of the results of DQ experiments and spin dynamics simulations demonstrated that the majority of individual chains possess completely adjacent re-entry structures at both T_c = 60 and ~0 °C, as well as indicated that a low polymer concentration, not kinetics, leads to cluster formations of single molecules in dilute solution. The changes in crystal habits from hexagonal shapes at T_c = 60 °C to rounded shapes at ~0 °C (kinetic roughness) are reasonably explained in terms of kinetically driven depositions of single molecule clusters on the growth front.

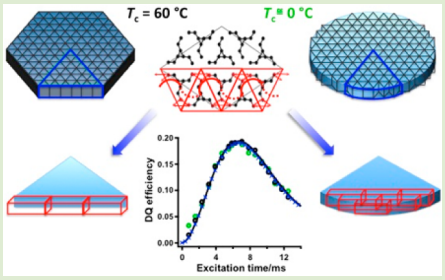

Polymer crystallization involves structural changes from random coils in the melt and solution states to folded chains with a typical thickness of about 5−20 nm in the bulk and single crystals, respectively. The crystallization of polymers driven by kinetics yields unique features in terms of crystal habits, lamellar thickness, and crystallinity, among other characteristics.[1−4] Figure 1A,B shows transmission electron microscopy (TEM) images of *i*PB1 single crystals, respectively, formed at T_c = 60 (spiral crystals) and ~0 °C. At T_c = 60 °C, the crystals show well-defined hexagonal crystals having a flat growth front at a side-plane length of about 2−3 μm and the crystal thickness was determined to be about 6.5 nm by atomic force microscopy (AFM; Figure S1), whereas rapid quenching at T_c = ~0 °C results in kinetically rounded crystals.[4]

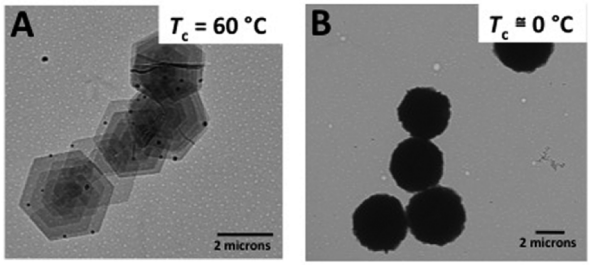

Figure 1. TEM images of *i*PB1 hexagonal and round single crystals crystallized at (A) T_c = 60 °C and (B) = ~0 °C, respectively.

The individual chain trajectory in solid crystals records the structural changes that occur during the crystallization process at different T_cs. Thereby, theoretical and experimental studies have focused on understanding the CF process and structure under different supercooling conditions.[5−17] According to Lauritzen−Hoffman (LH) theory,[5,6] the crystallization process is dominated by sequential stem deposition on the growth front. The competition between the secondary nucleation rate (i) and the growth rate (g) defines different regimes. Wide supercooling conditions are expected to lead to largely different CF structures. Conversely, Allegra et al. proposed a bundle model in which aggregates of 10−20 stems are produced by folding in the prestage of crystallization.[7] Muthukumar et al. developed an anisotropic aggregation model in which individual molecules generate folded structures in dilute solution in the prestage of crystallization.[8] It is suggested that depositions of clusters of folded and superfolded chains determine the resultant morphology. Various experimental approaches, including neutron scattering (NS),[9−12] IR,[13] surface decoration,[14] direct observation,[15,16] and force detection[17] of single molecules using AFM have been developed in the last four decades to identify CF structures in bulk as well as in single crystals. However, the quantitative analysis of the re-entrance sites of folded chains, n, and F in real polymer crystals remains challenging. Here, F is defined as $(\sum_{i=1}^{l}(n_i + 1))/N$, where l is the number of clusters consisting of adjacent re-entry structures per chain, n_i is the successive folding number of the ith cluster, and N is the number of all stems per chain. $\langle n \rangle$ is the mean successive CF number in l clusters (Figure S2).

Solid-state (SS) NMR is an excellent characterization tool for determining the three-dimensional structures of biomacromolecules[18] and small molecules,[19] as well as the local conformations of synthetic polymers.[20] Recently, we proposed

Received: April 3, 2014
Accepted: May 27, 2014
Published: May 29, 2014

   dx.doi.org/10.1021/mz500196s | *ACS Macro Lett.* 2014, 3, 556−559

a new strategy for characterizing the re-entrance sites of folded chains, $\langle n \rangle$, and F of synthetic polymers in bulk crystals using selective ^{13}C labeling and $^{13}C-^{13}C$ double-quantum (DQ) NMR.[21] DQ NMR relies on the $^{13}C-^{13}C$ dipolar coupling strength, which is inversely proportional to the third power of the internuclei distance r,[22] as well as the interacting spin numbers and the topology. In this work, we investigate detailed CF structures of ^{13}C 35% CH_3-labeled *i*PB1 (M_w = 37002 g/mol) solution-grown crystals blended with nonlabeled *i*PB1 (M_w = 36153 g/mol) generated by slow and rapid crystallization using DQ NMR. Based on the crystal thickness and M_w, we estimated the maximum CF number, n_{max}, to be 21. The effects of kinetics and polymer concentration on CF structures and the relationship between morphology and CF structures were determined.

Figure 2A shows the relaxation-filtered ($T_{1\rho H}$: ^1H spin–lattice relaxation in the rotating frame), ^{13}C single-quantum

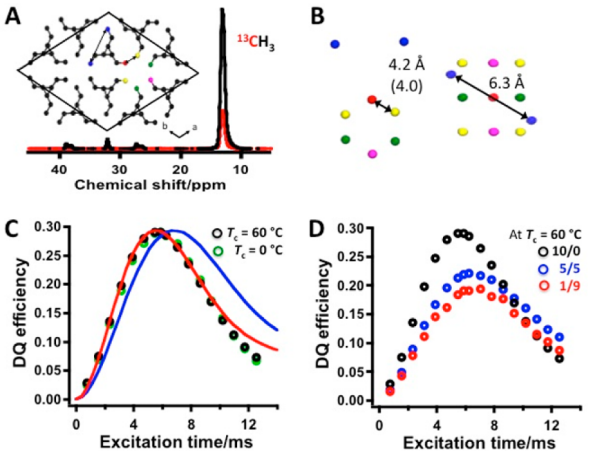

Figure 2. Chain-packing structure and DQ NMR of ^{13}C-labeled *i*PB1. (A) ^{13}C $T_{1\rho H}$-filtered DQ (red) and SQ (black) cross-polarization and magic-angle spinning (CPMAS) NMR spectra of 35% $^{13}CH_3$-labeled *i*PB1 form I measured at ambient temperature. The crystal structure, including the 11 colored ^{13}C CH_3 spin sites, was used in the chain-packing simulation. (B) Detailed coordinates of the 11-spin system in the (0 0 1) (left) and (1 $\bar{2}$ 0) planes (right). The shortest $^{13}C-^{13}C$ internuclear distances between neighboring stems (4.2 Å) and within a stem (6.3 Å), as determined by X-ray diffraction (XRD),[24] are shown as black arrows. (C) Experimental (open circles) and simulated ξ curves (solid lines) of $^{13}CH_3$-labeled form I *i*PB1. The red and blue curves are the calculated results based on chain-packing with a closest interstem r of 4.0 Å and an exponential T_2 of 21.0 ms or r = 4.2 Å and T_2 = 26.6 ms, respectively, as a function of τ_{ex}. (D) Dependence of the composition of ^{13}C-labeled *i*PB1 in the blends with nonlabeled chains (10/0 (black open circles), 5/5 (blue), and 1/9 (red)) on ξ as a function of τ_{ex}.

(SQ), and DQ NMR spectra of ^{13}C CH_3-labeled *i*PB1 form I single crystals with an excitation time (τ_{ex}) of 5.88 ms at ambient temperature. Figure 2C shows the DQ efficiency ξ of ^{13}C-labeled *i*PB1 form I at T_c = 60 °C (open black circles) and ~0 °C (greens) as a function of τ_{ex}. The apparent ξ can be described by $\xi(\tau_{eq}) = a(\tau_{eq}) \exp(-\tau_{eq}/T_2)$,[23] where the $a(\tau_{eq})$ term is the pure DQ efficiency based on the interacting spin numbers, spin topologies, and distances in the ^{13}C spin systems and T_2 is the incoherent relaxation. In principle, the apparent T_2 value includes unwanted contributions from chemical shift anisotropy, insufficient decoupling, rf., imperfection, and long-range dipolar interactions at lengths >7 Å that are not treated in the simulations. The packing structure of *i*PB1 form I[24] is depicted in Figure 2A, where the colored CH_3 carbons indicate those labeled with ^{13}C. Initially, the atomic coordinates reported in the literature[24] were used for the DQ build-up calculations. The model system consisted of a reference methyl carbon (colored red) plus the 10 closest surrounding carbons (8 interstem and 2 intrastem) at a distance of less than 6.4 Å (Figure 2A,B).[21] The 35% labeling ratio of methyl groups statistically produced different spin systems (number, distance, and topology) among the 11 sites, resulting in different build-up curves.

In these m spin systems, $a(\tau_{eq})$ is expressed as $a(\tau_{eq}) = (\Sigma w_{m-j} \cdot q_{m-j}(\tau_{eq}))P_m$, where $q_{m-j}(\tau_{eq})$ is an individual simulated curve for m spin systems (Figure S3), j is the spin topology of a given m spin system, and w_{m-j} is the probability of a given m spin system with spin topology j ($\Sigma_i w_{m-j} = 1$). Parameter P_m represents the probability of finding m spins among the 11 sites and is calculated using the equations $P_m = {}_{10}C_{m-1}(x)^{m-1}(1-x)^{10-(m-1)}$ and $\Sigma_{m=2}^{11} P = 1$, where ${}_{10}C_{m-1}$ and x are the combination and isotope labeling ratio, respectively. $\Sigma_8^{11} P_m$ was only ~2.5%, and the DQ curve for the six spin system was nearly identical to that for the seven spin system. Thus, the DQ curves for the spin interactions of more than eight spins are assumed to be the same as those for seven spins. Because the DQ curves are modulated by an apparent T_2 value, all possible spin interactions (shortest distance of 4.2 Å) with an apparent exponential T_2 of 26.6 ms result in one simulated DQ curve (blue curve in Figure 2C). The calculated curve shows a slightly slower build-up compared to the experimental curve. Therefore, the interstem distance is slightly reduced along the a and b axes equally. A simulated DQ build-up curve with a shortest internuclear distance of 4.0 Å and an exponential apparent T_2 value of 21.0 ms best fit the experimental results (red curve in Figure 2C). At T_c = ~0 °C (green open circles), the DQ build-up curve was the same as that observed at T_c = 60 °C. The obtained atomic coordinates and the T_2 value at T_c = 60 °C were used to analyze the CF structure in single crystals. Figure 2D shows the $^{13}C-^{13}C$ DQ build-up curves for *i*PB1 blends with different composition ratio (10/0, 5/5, and 1/9) of ^{13}C-labeled and nonlabeled *i*PB1 crystallized at 60 °C. ξ_{max} decreased from 0.29 at a composition of 10/0 to 0.22 at 5/5 and 0.19 at 1/9 concomitant with broadening of the build-up and relaxation curve. The observed compositional dependence of DQ intensity and curve shape indicates that the individual ^{13}C-labeled chains are separated from other labeled chains and are surrounded by nonlabeled chains. The majority of the dipolar coupling sources change from both intra- and interchains to intrachains only as the amount of labeled component decreases.

At T_c = 60 °C, we reasonably assumed that the flat growth front of the hexagonal shapes confines the two possible CF structures to an orientation parallel to that of the growth front. Figure 3A shows two models of possible CF structures in the hexagonal single crystals. In the CFI model, the chains are folded along one row, as illustrated in Figure 3A. In the CFII model, the chains alternately change folding directions and occupy two rows and thus the ^{13}C-labeled sites can interact more closely and produce a dense spin network, as depicted in Figure 3A. The arrows indicate growth directions. The DQ efficiencies of the ^{13}C-labeled chains in the blends with nonlabeled chains (mixing ratio of 1/9) calculated with $\langle n_{max} \rangle$ = 21 and F = 100% are shown with the experimental results in Figure 3B. In the CFI model (green solid curve), ξ_{max}

dx.doi.org/10.1021/mz500196s | *ACS Macro Lett.* 2014, 3, 556–559

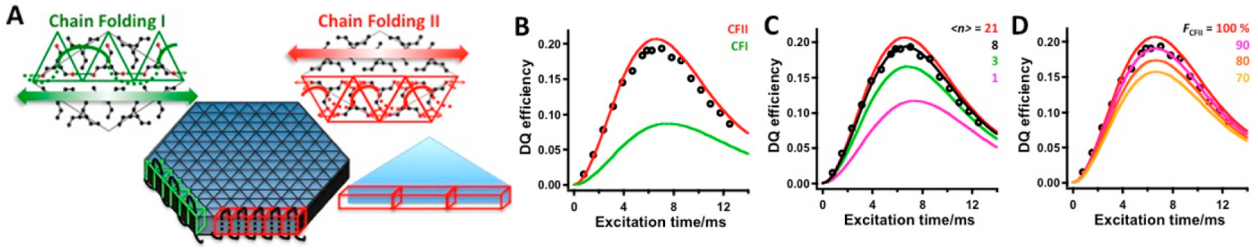

Figure 3. CF structures and DQ NMR of *i*PB1 at T_c = 60 °C. (A) Two possible CF models, CFI and CFII, for the hexagonal single crystal with a schematic representation of the CFII growth front with n = 21. (B) The experimental DQ build-up curves of ^{13}C-labeled *i*PB1 chains in the blends with nonlabeled chains (1/9) crystallized at 60 °C (black open circles) and the CFI and CFII curves calculated with $\langle n \rangle$ = 21 and F = 100%. (C) $\langle n \rangle$ and (D) F_{CFII} effects on the DQ curves calculated using the CFII model with F_{CFII} = 100% and $\langle n \rangle$ = 21, respectively, and the experimental results. In the latter, isolated stems contribute to DQ efficiency as the remaining fraction of 100 − F_{CFII}%. Note that all calculated results include statistical interchain effects.

was 0.09 at τ_{ex} = 7.45 ms, much lower than the experimentally obtained value. The calculated DQ build-up curve for the CFII model (red solid curve) exhibited a ξ_{max} value of 0.21 at τ_{ex} = 6.66 ms, which is very close to the experimental value (ξ_{max} = 0.19) in Figure 3B. $\langle n \rangle$ and F_{CFII} dependence of ξ under fixed F_{CFII} = 100% and $\langle n \rangle$ = 21, respectively, are illustrated in Figure 3C and D, respectively. Two limit structures of $\langle n \rangle$ = 8 (minimum) with F_{CFII} = 100% and $\langle n_{max} \rangle$ = 21 with F_{CFII} = 90% gave the best curve fits with the experimental results. In the latter, it was assumed that the remaining 10% of all stems contributed to the DQ curve as an isolated stem (see the later discussion of the isolated stem). The clusters consisting of single chains with $\langle n \rangle$ = 21 on the growth front are schematically illustrated in Figure 3A. These results are the first evidence for clusters consisting of single chains on the flat growth front of single crystals, consistent with the expected CF structure in well-defined single crystals based on the last half-century of research. Actually, individual chains might adopt not linear but box shapes due to superfolding. We further investigated DQ efficiency in box types of clusters on the basis of CFII model with superfolding number (sn) of 1 and 2. Adopting slightly lower F values of 80−85% can reproduce experimental data (Figure S4). Note that current DQ resolution is not high enough to determine whether whole chains adopt linear or box shapes of clusters. Determination of molecular shapes is a future subject in polymer characterization.

At T_c = ∼0 °C, the morphology of the solution-grown crystals is rounded due to rapid crystallization, during which stem deposition is expected to be governed by the secondary nucleation process ($i > g$) according to LH theory, where the kinetics would lead to smaller $\langle n \rangle$ and F values.[5,6] One plausible model, CF0, which is an isolated stem, is illustrated in Figure 4A, which results in a ξ_{max} value of only 0.04 (pink curve in Figure 4B). Note that the reference and 6 intrastem carbons were used for the isolated stem calculation. Two other models, CFIII and IV, where the niche separation is assumed to be similar to the stem width, and the effective CF directions would be radial in rounded crystals, are also shown in Figure 4A. The DQ efficiencies of the CFIII (orange) and CFIV (blue) curves were calculated assuming $\langle n \rangle$ = 5 and F = 50% (filled squares), $\langle n \rangle$ = 10 and F = 80% (filled circles), and $\langle n \rangle$ = 21 and F = 100% (solid curve) (Figure 4B), and the thicknesses of the single crystals prepared at ∼0 and 60 °C were assumed to be the same. For $\langle n \rangle$ = 21 and F = 100%, the CFIII and CFIV models gave ξ_{max} values of 0.13 at τ_{ex} = 7.45 ms and 0.20 at τ_{ex} = 6.66 ms, respectively. In the latter, ξ_{max} value is almost identical with the calculated ξ_{max} value under assumptions of

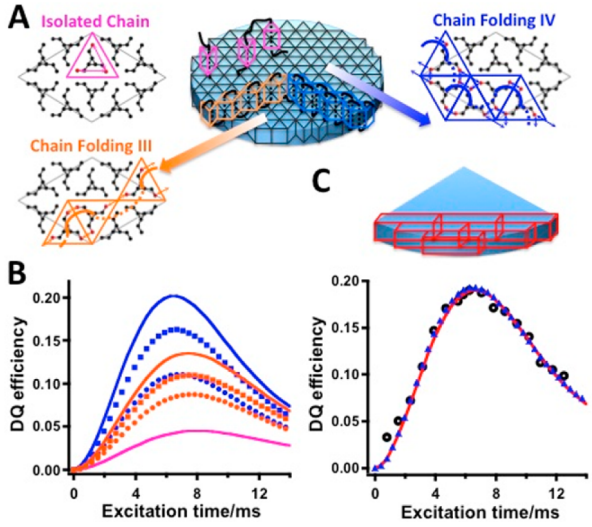

Figure 4. CF structures and DQ NMR of *i*PB1 at T_c = ∼0 °C. (A) Three possible CF models based on LH theory: isolated chain (CF0), CFIII, and CFIV. (B) The calculated DQ build-up curves using the CFIII (blue) and CFIV (orange) models with $\langle n \rangle$ = 21 and F = 100% (solid curve), $\langle n \rangle$ = 10 with F = 80% (filled squares), and $\langle n \rangle$ = 5 with F = 50% (filled circles), and CF0 (pink solid curve). (C) Experimental DQ build-up curves of the ^{13}C-labeled *i*PB1 chains in the blends with nonlabeled chains (1/9) (black open circles) and the CFII and CFIV DQ curves simulated with F_{CFII} = 90% and $\langle n \rangle$ = 21 (red solid curve) and F_{CFIV} = 95% and $\langle n \rangle$ = 21 (blue triangles), respectively. Note that all calculated results include statistical interchain effects. A schematic illustration of cluster depositions of single molecules using the CFII model is shown.

$\langle n \rangle$ = 21 and F = 100% using CFII, since two different models possess very similar spin topology. The experimental DQ build-up curves for the ^{13}C-labeled chains in the blend sample (open circles) prepared at T_c = ∼0 °C are shown in Figure 4C. Surprisingly, the experimental DQ curve exhibits a very high ξ_{max} value of 0.19, a value identical to that observed at T_c = 60 °C. Using the CFIV and II models, the calculated results for $\langle n \rangle$ = 21 and F_{CFIV} = 95% (blue triangles), and $\langle n \rangle$ = 21 and F_{CFII} = 90% (solid red curve), respectively, reproduce the experimental data (Figure 4C). Currently, the $\langle n \rangle$ and F values obtained using the CFIV and II models do not support sequential stem deposition dominated by kinetics and indicate that a low concentration of polymers leads to completely adjacent re-entry structures even under rapid quench conditions. Under the current proof of no kinetic effect on $\langle n \rangle$ and F values, the CFIV model driven by kinetics can be reasonably excluded as a

dx.doi.org/10.1021/mz500196s | *ACS Macro Lett.* 2014, 3, 556−559

plausible structure. Rather, the identical ξ_{max} values at T_c = ~0 and 60 °C simply support the CFII model, even under rapid crystallization. The identical CF structures obtained at T_c = 60 and ~0 °C indicate that there is no temperature regime for the CF process and that low concentration dominates the CF process in dilute solution and naturally reject CF process expected from LH theory.[5,6] Given the evidence for cluster formation at T_c = ~0 °C, cluster depositions driven by kinetics likely determine the resultant morphology. A plausible relationship between morphology and cluster deposition is schematically illustrated in Figure 4C. Depositions of CFII clusters on the growth front depending on T_c consequently determine the final morphology. The determined CF structures and relationship between crystal habits and molecular clusters across a wide supercooling are well consistent with those in aggregation model.[8]

In summary, we demonstrated that both high and low T_cs lead to cluster formations of single molecules via adjacent re-entry structures, whereas morphology is highly dependent on T_c. The results obtained indicate that low polymer concentrations, not kinetics, dominate the CF process in dilute solution and that cluster depositions driven by kinetics determine the resultant morphology at a given T_c. This novel approach will clarify how the kinetics, concentration, flexibility, and molecular weights influence CF structure in different polymer systems.

■ ASSOCIATED CONTENT

Supporting Information

Materials, experimental conditions, simulation result, AFM image, and ^{13}C DPMAS NMR spectra. This material is available free of charge via the Internet at http://pubs.acs.org.

■ AUTHOR INFORMATION

Corresponding Author

*E-mail: miyoshi@uakron.edu.

Notes

The authors declare no competing financial interest.

■ ACKNOWLEDGMENTS

This work was financially supported by the National Science Foundation (Grant No. DMR-1105829) and a UA start-up fund. We are greatly indebted to Dr. Jeffrey Quinn at Bridgestone America for the GPC measurements and Hyungin Lee at the University of Akron for the AFM measurements.

■ REFERENCES

(1) Cheng, S. Z. D.; Lotz, B. *Polymer* **2005**, *46*, 8662−8681.
(2) Strobl, G. *Prog. Polym. Sci.* **2006**, *31*, 398−442.
(3) Ungar, G.; Zhen, X. *Chem. Rev.* **2001**, *101*, 4157−4188.
(4) Tanzawa, Y. *Polymer* **1992**, *33*, 2659−2665.
(5) Lauritzen, J. I., Jr.; Hoffman, J. D. *J. Res. Natl. Bur. Stand., Sect. A* **1960**, *64*, 73−102.
(6) Hoffman, J. D.; Miller, R. L. *Polymer* **1997**, *38*, 3151−3212.
(7) Allegra, G.; Meille, S. V. *Adv. Polym. Sci.* **2005**, *191*, 87−135.
(8) Zhang, J.; Muthukumar, M. *J. Chem. Phys.* **2007**, *126*, 234904.
(9) Fisher, E. W. *Pure Appl. Chem.* **1978**, *50*, 1319−1341.
(10) Yoon, D. Y.; Flory, P. J. *Polymer* **1977**, *18*, 509−513.
(11) Sadler, D. M.; Keller, A. *Science* **1979**, *203*, 263−265.
(12) Zeng, X.; Ungar, G.; Spells, S. J.; King, S. M. *Macromolecules* **2005**, *38*, 7201−7204.
(13) Reddy, K. R.; Tashiro, K.; Sakurai, T.; Yamaguchi, N. *Macromolecules* **2008**, *41*, 9807−9813.
(14) Wittmann, J. C.; Lotz, B. *J. Polym. Sci., Polym. Phys. Ed.* **1985**, *23*, 205−226.
(15) Kumaki, J.; Kawauchi, T.; Yashima, E. *J. Am. Chem. Soc.* **2005**, *127*, 5788−5789.
(16) Mullin, N.; Hobbs, J. K. *Phys. Rev. Lett.* **2011**, *107*, 197801.
(17) Liu, K.; Song, Y.; Feng, W.; Liu, N.; Zhang, W.; Zhang, X. *J. Am. Chem. Soc.* **2011**, *133*, 3226−3229.
(18) Castellani, F.; Van Rossum, B.; Diehl, A.; Schubert, M.; Rehbein, K.; Oshikinat, H. *Nature* **2002**, *420*, 98−102.
(19) Nomura, K.; Takegoshi, K.; Terao, T.; Uchida, K.; Kainosho, M. *J. Am. Chem. Soc.* **1999**, *121*, 4064−4065.
(20) Schmidt-Rohr, K.; Hu, W.; Zumbylyadis, N. *Science* **1998**, *280*, 714−717.
(21) Hong, Y.; Miyoshi, T. *ACS Macro. Lett.* **2013**, *2*, 501−505.
(22) Abragam, A. *The Principles of Nuclear Magnetizm*; Oxford University Press: London, 1961.
(23) Karlsson, T.; Popham, J. M.; Long, J. R.; Oyler, N.; Drobny, G. P. *J. Am. Chem. Soc.* **2003**, *125*, 7394−7407.
(24) Natta, G.; Corradini, P.; Bassi, I. W. *Nuovo Cimento* **1960**, *15*, 52−67.